

# Magnetic Alloy/Ferrite Cavities

*H. Klingbeil*

Technische Universität Darmstadt, Darmstadt, Germany and  
GSI Helmholtzzentrum für Schwerionenforschung GmbH, Darmstadt, Germany

## Abstract

RF cavities loaded with magnetic alloy (MA) or ferrite ring cores are used in synchrotrons and storage rings if the maximum RF frequency is in the order of a few MHz. A simple model for the description of cavities of this type is derived. The most important parameters are defined, and some properties of the material and of the cavity are summarized. Different cavity configurations, development aspects, and several practical topics are covered. A few specific ferrite- and MA-loaded cavity systems are discussed as examples.

## Keywords

Ferrite ring core, magnetic alloy ring core, ferrite-loaded cavity, MA-loaded cavity, RF cavities for synchrotrons and storage rings, equivalent circuits for RF cavities.

## 1 Introduction

This contribution is based on the article “Ferrite cavities” [2] published in the CERN Report CERN-2011-007 under the CC BY 3.0 Attribution Licence [3] and on Section 4.1 of the textbook [4] which was re-published in 2022 as an open-access publication under the CC BY-NC-ND licence. The original content [5] has been modified and extended.

The revolution frequency of charged particles in synchrotrons or storage rings is usually lower than 10 MHz. Even if we consider comparatively small synchrotrons (e.g. like HIT in Heidelberg, Germany, or CNAO in Pavia, Italy, with about 20...25 m diameter, both used for tumor therapy), the revolution time will be greater than 200 ns since the particles cannot reach the speed of light. Because, according to  $f_{\text{RF}} = h \cdot f_{\text{R}}$ , the RF frequency is an integer multiple of the revolution frequency, the RF frequency will typically be lower than 10 MHz if only small harmonic numbers  $h$  are desired. For such an operating frequency, the spatial dimensions of a conventional RF resonator would be far too large to be used in a synchrotron. One possibility to solve this problem is to reduce the wavelength by filling the cavity with magnetic material. This is the basic idea of magnetic alloy (MA)-loaded cavities or ferrite-loaded cavities. Furthermore, this type of cavity offers a simple means to modify the resonant frequency in a wide range (typically up to a factor of 10) and in a comparatively short time (typically at least 10 ms cycle time [1]). The possibility to adjust the resonant frequency of a cavity to the desired operating frequency is called **tuning**. An alternative is the construction of an untuned cavity with sufficient bandwidth. In any case, MA- or ferrite-loaded cavities are suitable for ramped operation in a synchrotron.

## 2 Permeability of Magnetic Materials

In this contribution, all calculations are based on permeability quantities  $\mu$  for which  $\mu = \mu_{\text{r}}\mu_0$  holds. In material specifications, the relative permeability  $\mu_{\text{r}}$  is given which means that we have to multiply with  $\mu_0$  to obtain  $\mu$ . This comment is also valid for the incremental/differential permeability introduced in the following.

In RF cavities, only so-called **soft magnetic materials** which have a narrow hysteresis loop are of interest since their losses are comparatively low (in contrast to **hard magnetic materials** which are used

for permanent magnets<sup>1</sup>).

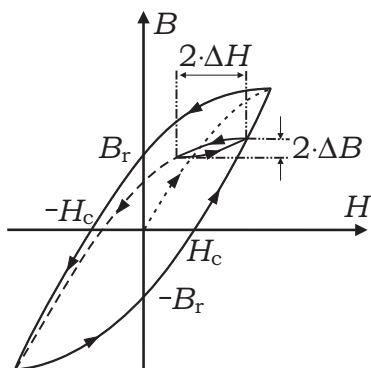


**Fig. 1:** Hysteresis loop.

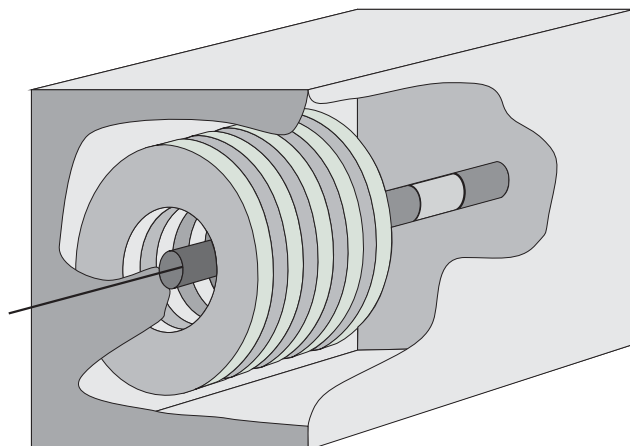


**Fig. 2:** Simplified 3D sketch of a ferrite- or MA-loaded cavity.

Figure 1 shows a **hysteresis loop** of a ferromagnetic material (not necessarily the full loop, but possibly a minor loop – see e.g. Ref. [6]). It is well-known that the hysteresis loop leads to a **residual induction**  $B_r$  if no magnetizing field  $H$  is present and that some **coercive magnetizing field**  $H_c$  is needed to set the induction  $B$  to zero.<sup>2</sup>

Let us now assume that some cycles of the larger hysteresis loop in Fig. 1 have already passed and that  $H$  is currently increasing. We now stop to increase the magnetizing field  $H$  in the upper right part of the diagram. Then,  $H$  is decreased by a much smaller amount  $2 \cdot \Delta H$ , afterwards increased again by that amount  $2 \cdot \Delta H$ , and so forth<sup>3</sup>. As the diagram shows, this procedure will lead to a much smaller hysteresis loop where  $B$  changes by  $2 \cdot \Delta B$ . We may therefore define a **differential** or **incremental permeability**<sup>4</sup>

$$\mu_{\Delta} = \frac{\Delta B}{\Delta H}$$

which describes the slope of the local hysteresis loop. It is this quantity  $\mu_{\Delta}$  which is relevant for RF applications. One can see that  $\mu_{\Delta}$  can be decreased by increasing the DC component of  $H$  thereby driving the material closer to saturation. Since  $H$  is generated by currents, one speaks of a **bias current** that is applied in order to shift the **operating point** to higher inductions  $B$  leading to a lower differential permeability  $\mu_{\Delta}$ .

The hysteresis loops and the AC permeability of ferromagnetic materials can be described in a phenomenological way by the so-called **Preisach model** (Ref. [7]) or similar models [8]. Unfortunately,

<sup>1</sup>No strict separation exists between hard and soft magnetic materials.

<sup>2</sup>The quantities  $B_r$  and  $H_c$  are usually defined for the full hysteresis loop with saturation, but they can also be defined for symmetrical minor loops.

<sup>3</sup>The factor of 2 was assumed in order to have the same total change of  $2 \cdot \Delta H$  as in the equation

$$H_{AC}(t) = \Delta H \cos(\omega t)$$

which is usually used for harmonic oscillations.

<sup>4</sup>In a strict sense, the differential permeability is the limit

$$\mu_{\Delta} = \frac{dB}{dH}$$

for  $\Delta H, \Delta B \rightarrow 0$ .

the material properties are even more complicated since they are also frequency-dependent. One usually uses the **complex permeability**

$$\boxed{\underline{\mu} = \mu'_s - j\mu''_s} \quad (1)$$

to describe losses (hysteresis loss, eddy current loss and residual loss). The parameters  $\mu'_s$  and  $\mu''_s$  are frequency-dependent. In the following, we will assume that the complex permeability  $\underline{\mu}$  describes the material behavior in rapidly alternating fields as the above-mentioned real quantity  $\mu_\Delta$  does when a biasing field  $H_{\text{bias}}$  is present. However, we will omit the index  $\Delta$  for the sake of simplicity.

### 3 Magneto-Quasistatic Analysis of an MA/Ferrite Cavity

In this section, we will see that a ferrite- or MA-loaded cavity may roughly be regarded as a transformer whose primary coil consists of only one winding fed by an RF power source and where the beam interaction with the cavity can be described by a secondary coil. Consequently, some conclusions that are valid for transformers are also valid here. For example, the cavity will not work properly if the frequency is too low because the reactance (product of inductance and angular frequency) will be too small in comparison with the ohmic parts thereby decreasing the transformation ratio. If the frequency becomes too large flux leakage and distributed effects will become important, so that a simple magneto-quasistatic analysis is no longer possible. Hence, an optimum operating frequency range can be specified for an MA- or ferrite-loaded cavity similar to a transformer taking the material properties and the geometry into account. It is assumed without further notice that the considered frequency belongs to this optimum frequency range.

Figure 2 shows the main elements of a ferrite-loaded cavity. The conductive beam pipe is interrupted by a **ceramic gap**. This gap ensures that the beam pipe may still be evacuated but it allows a voltage  $V_{\text{gap}}$  to be induced in longitudinal direction. Several MA or ferrite **ring cores** are mounted in a concentric way around beam and beam pipe (five ring cores are drawn here as an example). The whole cavity is surrounded by a metallic housing which is connected to the beam pipe.

Figure 3 shows a cross-section through the cavity. The dotted line represents the beam which is located in the middle of the metallic beam pipe (for analyzing the influence of the beam current, this dotted line is regarded as a part of a circuit that closes outside the cavity, but this is not relevant for understanding the basic operation principle). The ceramic gap has a parasitic capacitance, further distributed capacitances are always present, and additional lumped-element capacitors are often connected in parallel to the gap — leading to the overall capacitance  $C$ . Starting at the generator port located at the bottom of the figure, an inductive coupling loop surrounds the ring core stack. This loop was not shown in Fig. 2.

Due to the cross-section approach, we get a wire model of the cavity with ideal wires representing the cavity housing. This is sufficient for the practical analysis, but one should remember that the currents are distributed in reality.

In the following, voltages, currents, field and flux quantities will be represented by phasors, i.e. complex amplitudes/peak values for a given frequency  $f = \omega/2\pi$ . For a quantity  $X$  in time domain, we write  $\underline{X}$  for the phasor in frequency domain. The function  $X(t)$  can be reconstructed by means of the complex function  $\underline{X} = \underline{X}e^{j\omega t}$  according to  $X(t) = \text{Re}\{\underline{X}\} = \text{Re}\{\underline{X}e^{j\omega t}\}$ .

Let us consider the coupling loop contour in Fig. 3 which surrounds the lower left ring core stack cross-section. Based on Maxwell's second equation in the time domain (Faraday's law)

$$\oint_{\partial A} \vec{E} \cdot d\vec{r} = - \int_A \dot{\vec{B}} \cdot d\vec{A}$$

we find

$$\hat{V}_{\text{gen}} = +j\omega\hat{\Phi}_{\text{m,tot}}$$

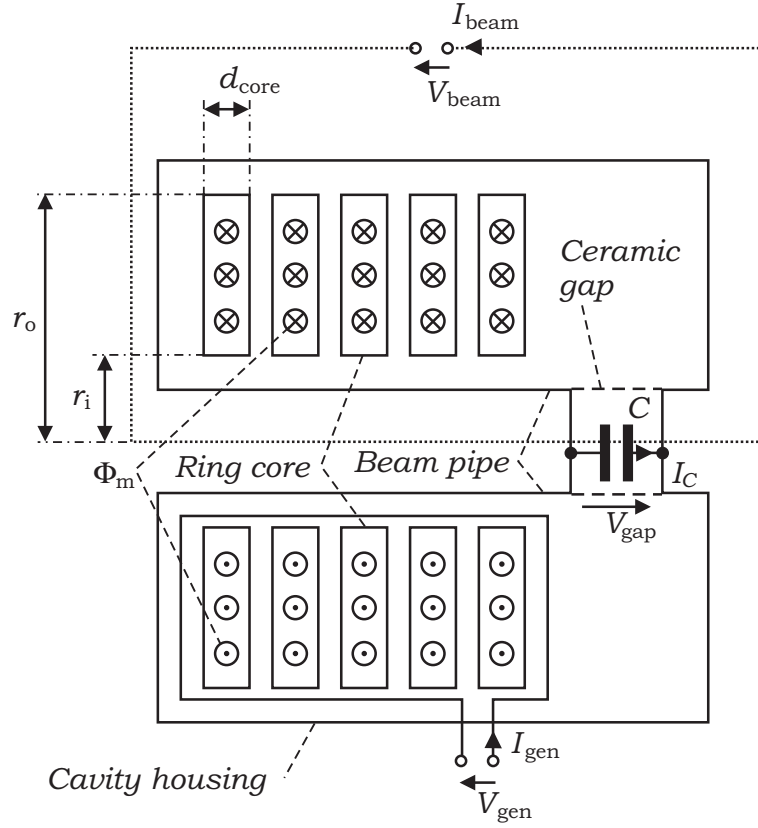


**Fig. 3:** Simplified wire model of a ferrite or MA cavity.

as the dependence of the generator voltage on the magnetic flux in the frequency domain. If we now use the complete lower cavity half or the beam current contour as integration paths, one obtains

$$\hat{V}_{\text{gap}} = +j\omega\hat{\Phi}_{\text{m,tot}}, \quad \hat{V}_{\text{beam}} = +j\omega\hat{\Phi}_{\text{m,tot}} \quad \Rightarrow \quad \hat{V}_{\text{beam}} = \hat{V}_{\text{gap}} = \hat{V}_{\text{gen}}. \quad (2)$$

Here we assumed that the stray field  $B$  in the air regions is negligible in comparison with the field inside the ring cores (due to their high permeability). For negligible displacement current we have Maxwell's first equation (Ampère's law)

$$\oint_{\partial A} \vec{H} \cdot d\vec{r} = \int_A \vec{J} \cdot d\vec{A}.$$

We use a concentric circle with radius  $\rho$  around the beam axis as integration path:

$$H \, 2\pi\rho = I_{\text{tot}}.$$

In the frequency domain, this leads to

$$\hat{B} = \mu \frac{\hat{I}_{\text{tot}}}{2\pi\rho} \quad (3)$$

with

$$\hat{I}_{\text{tot}} = \hat{I}_{\text{gen}} - \hat{I}_C - \hat{I}_{\text{beam}}. \quad (4)$$

For the flux through one single ring core we get

$$\hat{\Phi}_{\text{m},1} = \int \hat{B} \cdot d\vec{A} = d_{\text{core}} \int_{r_i}^{r_o} \hat{B} \, d\rho = \frac{d_{\text{core}}\mu\hat{I}_{\text{tot}}}{2\pi} \ln \frac{r_o}{r_i}.$$

With the complex permeability  $\underline{\mu} = \mu'_s - j\mu''_s$  and assuming that  $N$  ring cores are present, Eq. (2) provides

$$\hat{V}_{\text{gap}} = j\omega \hat{\Phi}_{\text{m,tot}} = j\omega N \hat{\Phi}_{\text{m},1} = j\omega \frac{Nd_{\text{core}}(\mu'_s - j\mu''_s) \hat{I}_{\text{tot}}}{2\pi} \ln \frac{r_o}{r_i}.$$

Therefore, we obtain

$$\hat{V}_{\text{gap}} = \hat{I}_{\text{tot}}(j\omega L_s + R_s) = \hat{I}_{\text{tot}} Z_s, \quad (5)$$

if

$$Z_s = \frac{1}{Y_s} = j\omega L_s + R_s, \quad (6)$$

$$\boxed{L_s = \frac{Nd_{\text{core}}\mu'_s}{2\pi} \ln \frac{r_o}{r_i}}, \quad \boxed{R_s = \omega \frac{Nd_{\text{core}}\mu''_s}{2\pi} \ln \frac{r_o}{r_i} = \omega \frac{\mu''_s}{\mu'_s} L_s = \frac{\omega L_s}{Q}} \quad (7)$$

are defined. Here,

$$Q = \frac{\mu'_s}{\mu''_s} = \frac{1}{\tan \delta_\mu} \quad (8)$$

is the **quality factor** (or **Q factor**) of the ring core material. Using Eq. (4) we find:

$$\hat{V}_{\text{gap}} Y_s = \hat{I}_{\text{tot}} = \hat{I}_{\text{gen}} - \hat{I}_{\text{beam}} - \hat{V}_{\text{gap}} j\omega C \Rightarrow \hat{V}_{\text{gap}} = \frac{\hat{I}_{\text{gen}} - \hat{I}_{\text{beam}}}{Y_s + j\omega C} = Z_{\text{tot}}(\hat{I}_{\text{gen}} - \hat{I}_{\text{beam}}) \quad (9)$$

This equation corresponds to the equivalent circuit shown in Fig. 4. In the last step, we defined  $Y_{\text{tot}} = 1/Z_{\text{tot}} = Y_s + j\omega C$ . In literature one often finds a different version of Eq. (9) where  $\hat{I}_{\text{beam}}$  has the same sign as  $\hat{I}_{\text{gen}}$ . This corresponds to both currents having the same direction (flowing into the circuits in Figs. 4 and 5). In any case, one has to make sure that the correct phase between beam current and gap voltage is established.

Assuming that the gap voltage is given by  $V_{\text{gap}}(t) = \hat{V}_{\text{gap}} \sin(\omega_{\text{RF}}t)$ , the bunches will be located at  $t = 0, \pm T_{\text{RF}}, \pm 2T_{\text{RF}}, \dots$  if the stationary case without acceleration is considered (operation with positively charged particles below transition energy). Therefore, the fundamental harmonic of the beam current will be proportional to  $\cos(\omega_{\text{RF}}t)$  which corresponds to a  $90^\circ$  phase shift between  $V_{\text{gap}}$  and  $I_{\text{beam}}$ . For low beam currents and for a cavity that is tuned to resonance, the phase of the gap voltage is equal to the phase of the generator current. For higher beam currents, however, not only the generator current, but also the beam current will have an influence on the gap voltage due to the **beam impedance**  $Z_{\text{tot}}$  as one sees in Eq. (9) and in Fig. 4. This phenomenon is called **beam loading**.

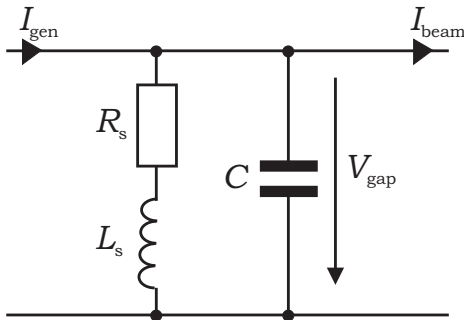


**Fig. 4:** Series equivalent circuit.

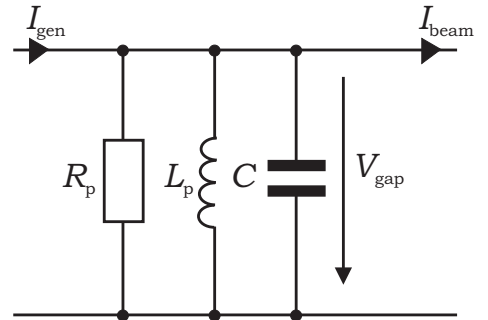


**Fig. 5:** Parallel equivalent circuit.

#### 4 Parallel and Series Lumped Element Circuit

Assuming frequency-dependent values<sup>5</sup>  $R_s$ ,  $L_s$ ,  $R_p$ ,  $L_p$ , it is possible to convert the lumped element circuit shown in Fig. 4 into a parallel circuit as shown in Fig. 5. The admittance of both circuits shall be equal:

$$Y_{\text{tot}} = j\omega C + \frac{1}{R_s + j\omega L_s} = j\omega C + \frac{1}{R_p} + \frac{1}{j\omega L_p} \Rightarrow \frac{R_s - j\omega L_s}{R_s^2 + (\omega L_s)^2} = \frac{1}{R_p} + \frac{1}{j\omega L_p}$$

A comparison of real and imaginary part yields

$$\boxed{R_p = \frac{R_s^2 + (\omega L_s)^2}{R_s}}, \quad \boxed{\omega L_p = \frac{R_s^2 + (\omega L_s)^2}{\omega L_s}} \quad (10)$$

$$\Rightarrow R_p R_s = (\omega L_p)(\omega L_s). \quad (11)$$

For the inverse relation, we write the first Eq. (10) in the form  $(\omega L_s)^2 = R_s(R_p - R_s)$  and use this result in Eq. (11):

$$\omega L_p \sqrt{R_s(R_p - R_s)} = R_s R_p \Rightarrow (\omega L_p)^2 (R_p - R_s) = R_s R_p^2 \Rightarrow \boxed{R_s = \frac{(\omega L_p)^2}{R_p^2 + (\omega L_p)^2} R_p} \quad (12)$$

With this formula, Eq. (11) leads to

$$\boxed{\omega L_s = \frac{R_p}{\omega L_p} R_s = \frac{R_p^2}{R_p^2 + (\omega L_p)^2} \omega L_p}.$$

Since it is suitable to use both types of lumped element circuit, it is also convenient to define the complex permeability  $\underline{\mu}$  in a parallel form:

$$\boxed{\frac{1}{\underline{\mu}} = \frac{1}{\mu'_p} + j \frac{1}{\mu''_p}}. \quad (13)$$

This is an alternative representation for the series form shown in Eq. (1) which leads to

$$\frac{1}{\underline{\mu}} = \frac{\mu'_s + j\mu''_s}{\mu'^2_s + \mu''^2_s}.$$

Comparing the real and imaginary parts of the last two equations, we find

$$\mu'_p = \frac{\mu'^2_s + \mu''^2_s}{\mu'_s}, \quad \mu''_p = \frac{\mu'_s \mu''_s}{\mu''_s} \Rightarrow \mu'_p \mu'_s = \mu''_p \mu''_s. \quad (14)$$

Together with Eqs. (7), (8), and (11) we conclude:

$$\boxed{Q = \frac{\mu'_s}{\mu''_s} = \frac{\omega L_s}{R_s} = \frac{R_p}{\omega L_p} = \frac{\mu''_p}{\mu'_p}}. \quad (15)$$

<sup>5</sup>Even if all circuit elements are assumed to be frequency-independent, both equivalent circuits lead to a similar impedance curve in the vicinity of the resonance frequency.

With these expressions, we may write Eq. (14) in the form

$$\boxed{\mu'_p = \mu'_s \left(1 + \frac{1}{Q^2}\right)}, \quad \boxed{\mu''_p = \mu''_s (1 + Q^2)}. \quad (16)$$

If we use  $Q = \omega L_s / R_s$  from Eq. (15), we may rewrite Eq. (10) in the form

$$\boxed{R_p = R_s(1 + Q^2)}, \quad \boxed{L_p = L_s \left(1 + \frac{1}{Q^2}\right)}. \quad (17)$$

By combining Eqs. (17) and (7) we find

$$R_p = (1 + Q^2) \omega \frac{Nd_{\text{core}} \mu''_s}{2\pi} \ln \frac{r_o}{r_i}.$$

With the help of Eqs. (15) and (16) one gets

$$R_p = \omega \frac{Nd_{\text{core}} \mu''_p}{2\pi} \ln \frac{r_o}{r_i} = \omega \frac{Nd_{\text{core}} \mu'_p Q}{2\pi} \ln \frac{r_o}{r_i} = Nd_{\text{core}} \mu'_p Q f \ln \frac{r_o}{r_i}.$$

This shows that  $R_p$  is proportional to the product  $\mu'_p Q f$  which is a material property. The other parameters refer to the geometry. Therefore, the manufacturers of ferrite cores or MA cores sometimes specify the  $\mu_r \mathbf{Qf}$  **product** (for the sake of simplicity, we define<sup>6</sup>  $\mu_r := \mu'_{p,r}$ ).

For  $Q \geq 5$  (typically fulfilled for ferrites), we may use the approximations

$$R_p \approx R_s Q^2, \quad L_p \approx L_s, \quad \mu'_p \approx \mu'_s, \quad \mu''_p \approx \mu''_s Q^2 \quad (18)$$

which then have an error of less than 4 %.

## 5 Frequency Dependence of Material Properties

As an example, the frequency dependence of the permeability is shown in Figs. 6 and 7 for the special ferrite material Ferroxcube 4 assuming small magnetic RF fields without biasing. All the data presented for this material are taken from [9]. It is obvious that the behavior depends significantly on the choice of the material. Without biasing, a constant  $\mu'_s \approx \mu'_p$  may only be assumed up to a certain frequency (see Fig. 6). Increasing the frequency from 0 upwards, the Q factor will decrease (compare Figs. 6 and 7). Figure 8 shows the resulting frequency dependence of the  $\mu_r Q f$  product.

If the magnetic RF field is increased, both  $Q$  and  $\mu_r Q f$  will decrease in comparison with the diagrams in Figs. 6-8. The effective incremental permeability  $\mu_r$  will increase for rising magnetic RF fields as one can see by interpreting Fig. 1. Therefore, it is important to consider the material properties under realistic operating conditions (the maximum RF B-field for ferrites is usually in the order of 10...20 mT).

If biasing is applied, the  $\mu_r Q f$  curve shown in Fig. 8 will be shifted to the lower right side; this effect may approximately compensate the increase of  $\mu_r Q f$  with frequency [9]. Therefore, the  $\mu_r Q f$  product may sometimes approximately be regarded as a constant if biasing is used to keep the cavity at resonance for all frequencies under consideration.

<sup>6</sup>Here, the index  $r$  again denotes the relative permeability, i.e.  $\mu'_{p,r} = \mu'_p / \mu_0$

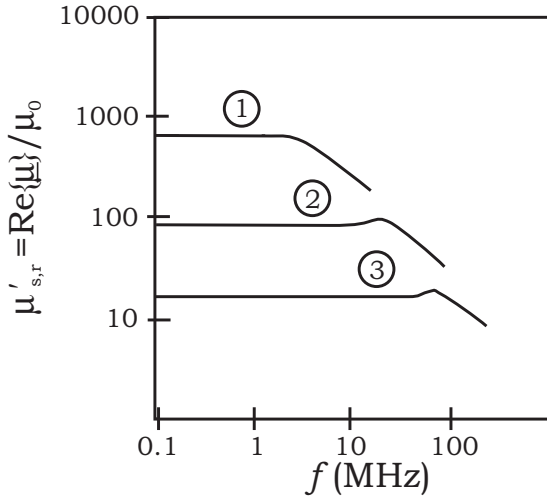


**Fig. 6:**  $\mu'_{s,r}$  versus frequency for three different types of ferrite material (1: Ferrocube 4A, 2: Ferrocube 4C, 3: Ferrocube 4E). Data adopted from [9].

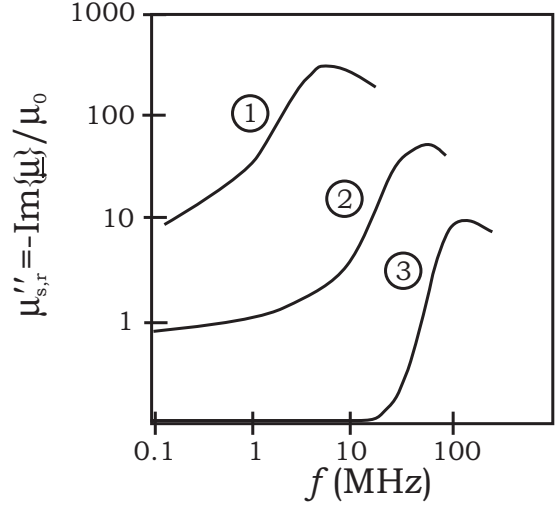


**Fig. 7:**  $\mu''_{s,r}$  versus frequency for three different types of ferrite material (1: Ferrocube 4A, 2: Ferrocube 4C, 3: Ferrocube 4E). Data adopted from [9].

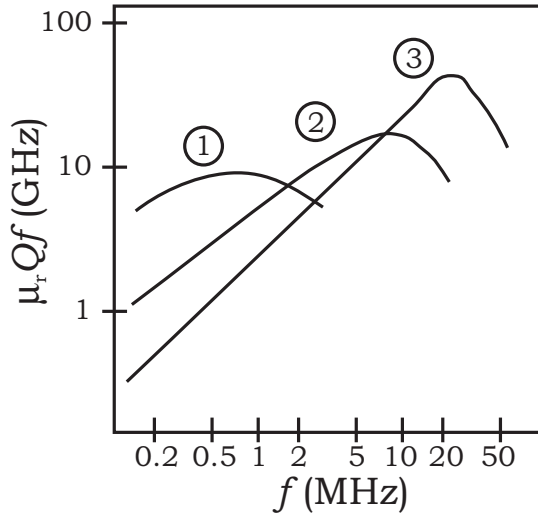


**Fig. 8:**  $\mu'_{s,r} Q f$  product versus frequency for three different types of ferrite material (1: Ferrocube 4A, 2: Ferrocube 4C, 3: Ferrocube 4E). Please note that  $\mu_r := \mu'_{p,r} \approx \mu'_{s,r}$  holds due to Eq. (18). No bias field is present, and small magnetic RF field amplitudes are assumed. Data adopted from [9].

## 6 Quality Factor of the Cavity

The quality factor of the equivalent circuit shown in Fig. 5 is obtained if the **resonant (angular) frequency**

$$\omega_{\text{res}} = 2\pi f_{\text{res}} = \frac{1}{\sqrt{L_p C}}$$

is inserted into Eq. (15):

$$Q_p = R_p \sqrt{\frac{C}{L_p}}.$$

In general, all parameters  $\mu'_s, \mu''_s, \mu'_p, \mu''_p, R_s, L_s, R_p, L_p, Q$  and  $Q_p$  are frequency-dependent. It depends on the material whether the parallel or the series lumped element circuit is the better representation in the sense that its parameters may be regarded as approximately constant in the relevant operating range. In the following, we will use the parallel representation.

We briefly show that  $Q_p$  is in fact the quality factor defined by  $Q_p = \omega \overline{W}_{\text{tot}} / \overline{P}_{\text{loss}}$ , where  $\overline{W}_{\text{tot}}$  is the stored energy and  $\overline{P}_{\text{loss}}$  is the power loss (both time-averaged):

$$\overline{P}_{\text{loss}} = \frac{|\hat{V}_{\text{gap}}|^2}{2R_p} \quad (19)$$

$$\overline{W}_{\text{el}} = \frac{1}{4} C |\hat{V}_{\text{gap}}|^2, \quad \overline{W}_{\text{magn}} = \frac{1}{4} L_p |\hat{I}_L|^2 = \frac{1}{4} L_p \frac{|\hat{V}_{\text{gap}}|^2}{\omega^2 L_p^2} = \frac{|\hat{V}_{\text{gap}}|^2}{4\omega^2 L_p}.$$

At resonance, we have  $\overline{W}_{\text{el}} = \overline{W}_{\text{magn}}$  which leads to

$$Q_p = 2\omega \frac{\overline{W}_{\text{el}}}{\overline{P}_{\text{loss}}} = 2\omega \frac{R_p C}{2} = R_p \sqrt{\frac{C}{L_p}}$$

as expected. The parallel resistor  $R_p$  defined by Eq. (19) is sometimes called **shunt impedance**. Please note that different definitions for the shunt impedance exist in literature. Sometimes, especially in the LINAC community, the shunt impedance is defined as two times  $R_p$  (see Ref. [10]).

## 7 Impedance of the Cavity

According to Fig. 5, the impedance of the cavity

$$Z_{\text{tot}} = \frac{1}{\frac{1}{R_p} + j\left(\omega C - \frac{1}{\omega L_p}\right)} = \frac{\sqrt{\frac{L_p}{C}}}{\frac{1}{R_p} \sqrt{\frac{L_p}{C}} + j\left(\omega \sqrt{L_p C} - \frac{1}{\omega \sqrt{L_p C}}\right)}$$

may be written as

$$Z_{\text{tot}} = \frac{\frac{R_p}{Q_p}}{\frac{1}{Q_p} + j\left(\frac{\omega}{\omega_{\text{res}}} - \frac{\omega_{\text{res}}}{\omega}\right)} \Rightarrow Z_{\text{tot}} = \frac{R_p}{1 + j Q_p \left(\frac{\omega}{\omega_{\text{res}}} - \frac{\omega_{\text{res}}}{\omega}\right)}. \quad (20)$$

The Laplace transformation yields

$$Z_{\text{tot}}(s) = \frac{R_p}{1 + s \frac{Q_p}{\omega_{\text{res}}} + \frac{Q_p \omega_{\text{res}}}{s}} = \frac{R_p \frac{\omega_{\text{res}} s}{Q_p}}{s \frac{\omega_{\text{res}}}{Q_p} + s^2 + \omega_{\text{res}}^2}, \quad (21)$$

which may be found in literature (see Refs. [11, 12]) in the form

$$Z_{\text{tot}}(s) = \frac{2R_p \sigma s}{s^2 + 2\sigma s + \omega_{\text{res}}^2}$$

if  $\sigma = \frac{\omega_{\text{res}}}{2Q_p}$  is defined. As shown in Ref. [4], Eq. (20) leads to the 3 dB bandwidth of the cavity provided that  $R_p$  and  $Q_p$  are frequency-independent:

$$Q_p = \frac{\omega_{\text{res}}}{\Delta\omega_{3\text{dB}}} = \frac{f_{\text{res}}}{\Delta f_{3\text{dB}}}.$$

## 8 Length of the Cavity

In the previous sections, we assumed that the ring cores can be regarded as lumped-element inductors and resistors. This is of course only true if the cavity is short in comparison with the wavelength.

As an alternative to the transformer model introduced above, one may therefore use a coaxial transmission line model [13]. For example, the section of the cavity that is located on the left side of the ceramic gap in Fig. 3 may be interpreted as a coaxial line that is homogeneous in longitudinal direction and that has a short-circuit at the left end. The cross section consists of the magnetic material of the ring cores, air between the ring cores and the beam pipe, and air between the ring cores and the cavity housing. This is of course an idealization since cooling disks, conductors and other air regions are neglected. Taking the SIS18 cavity at GSI as an example, the ring cores have  $\mu_r = 28$  at an operating frequency of 2.5 MHz. They have a relative dielectric constant of 10...15, but this is reduced to an effective value of  $\varepsilon_{r,\text{eff}} = 1.8$  since the ring cores do not fill the full cavity cross section. These values lead to a wavelength of  $\lambda = 16.9$  m. Since 64 ring cores with a thickness of 25 mm are used, the effective length of the magnetic material is 1.6 m = 0.095  $\lambda$  (which corresponds to a phase of 34°). In this case, the transmission line model leads to deviations of less than 10 % with respect to the lumped-element model.

The transmission line model makes it understandable why the MA- or ferrite-loaded cavity is sometimes referred to as a **shortened quarter-wavelength resonator**.

Of course, one may also use more detailed models where subsections of the cavity are modeled as lumped elements. In this case, computer simulations can be performed to calculate the overall impedance. In case one is interested in resonances which may occur at higher operating frequencies, one should perform full electromagnetic simulations.

In any case, one should always remember that some parameters are difficult to determine, especially the permeability of the ring core material under different operating conditions. This uncertainty may lead to larger errors than simplifications of the model. Measurements of full-size ring cores in the requested operating range are inevitable when a new cavity is developed [14]. Also parameter tolerances due to the manufacturing process have to be taken into account.

In general, one should note that the total length and the dimensions of the cross-section of the ferrite or MA cavity are not determined by the wavelength as for a conventional RF cavity. For example, the SIS18 ferrite cavity has a length of 3 m flange-to-flange although only 1.6 m are filled with magnetic material. This provides space for the ceramic gap, the cooling disks and further devices like the bias current bars. In order to avoid resonances at higher frequencies of the operating range, one should not waste too much space, but there is no exact size of the cavity housing that results from the electromagnetic analysis.

## 9 Differential Equation and Cavity Filling Time

The equivalent circuit shown in Fig. 5 was derived in the frequency domain. As long as no parasitic resonances occur, this equivalent circuit may be generalized. Therefore, we may also analyze it in the time domain (allowing only slow tuning changes of  $L_p$  and  $R_p$  with time) leading to

$$\ddot{V}_{\text{gap}} + \frac{2}{\tau} \dot{V}_{\text{gap}} + \omega_{\text{res}}^2 V_{\text{gap}} = \frac{1}{C} \frac{d}{dt} (I_{\text{gen}} - I_{\text{beam}}). \quad (22)$$

Here we used the definition

$$\tau = 2R_p C.$$

The product  $R_p C$  is also present in the expression for the quality factor:

$$Q_p = R_p \sqrt{\frac{C}{L_p}} = \frac{R_p C}{\sqrt{L_p C}} = \frac{1}{2} \tau \omega_{\text{res}} \quad \Rightarrow \quad \tau = \frac{2Q_p}{\omega_{\text{res}}} = \frac{Q_p}{\pi f_{\text{res}}}$$

Under the assumption  $\omega_{\text{res}} > \frac{1}{\tau}$  ( $Q_p > \frac{1}{2}$ ), the ansatz  $V_{\text{gap}} = V_0 e^{\alpha t}$  (with a complex constant  $\alpha$ ) for the homogeneous solution of Eq. (22) actually leads to  $\alpha = -\frac{1}{\tau} \pm j\omega_d$  with the exponential decay time  $\tau$  and the oscillation frequency

$$\omega_d = \omega_{\text{res}} \sqrt{1 - \frac{1}{(\tau \omega_{\text{res}})^2}} = \omega_{\text{res}} \sqrt{1 - \frac{1}{4Q_p^2}}.$$

This yields  $\omega_d \approx \omega_{\text{res}}$  even for moderately high  $Q_p > 2$  (error less than 4 %). Sometimes, the resonant frequency  $\omega_{\text{res}}$  is called the **undamped natural frequency** whereas  $\omega_d$  is called the **damped natural frequency**.

The time  $\tau$  is the time constant for the cavity which also determines the **cavity filling time**. Furthermore, the time constant  $\tau$  is relevant for amplitude and phase jumps of the cavity (see Ref. [15]).

Sometimes, especially in the LINAC community, the cavity filling time is defined as  $Q_p/\omega_{\text{res}}$  (one half of our definition, Ref. [10]) in order to specify the energy decay instead of the field strength or voltage decay.

## 10 Power Amplifier

Up to now, the Q factor of the cavity was called  $Q_p$ . What we did not mention so far is that the Q factor of the cavity itself is the so-called **'unloaded Q factor'**. From now on, this unloaded Q factor will be denoted as  $Q_{p,0}$ . In accordance with this, the parallel resistor will be denoted as  $R_{p,0}$ . The reason for this is the following: An RF power amplifier that feeds the cavity may often be represented by a voltage-controlled current source (e.g. in the case of a tetrode amplifier). The impedance of this current source will be connected in parallel to the equivalent circuit of the cavity thereby reducing the ohmic part  $R_p$  according to  $R_p = R_{p,0} || R_{\text{gen}}$  (see Fig. 9, Section 14). Therefore, the **loaded Q factor**  $Q_p$  will usually be reduced in comparison with the unloaded Q factor  $Q_{p,0}$  provided that  $C_{\text{gen}}$  is not too large.

The formulas that were derived for the parallel equivalent circuit are valid for both cases, the cavity alone and the combination of cavity and amplifier. This is the reason why they were based on  $R_p$ .

It has to be emphasized that for MA- or ferrite-loaded cavities 50  $\Omega$  impedance matching is not necessarily used in general. The cavity impedance is usually in the order of a few hundred ohms or a few kilo-ohms. Therefore, it is often more suitable to directly connect the tetrode amplifier to the cavity. Impedance matching is not mandatory if the amplifier is located close to the cavity. Short cables have to be used since they contribute to the overall impedance. Cavity and RF power amplifier must be considered as one unit; they cannot be developed separately because their impedance curves influence each other.

## 11 Cooling

Both, the power amplifier and the ring cores need active cooling. Depending on the operating conditions (e.g. CW or pulsed operation), **forced air cooling** may be sufficient for the ring cores or **water cooling** may be required. Avoiding direct contact of the ferrite ring cores with water, **cooling disks** in-between the cores may be used. In this case, one has to make sure that the thermal contact between cooling disks and ferrites is good. For MA ring cores, direct water cooling [16] or direct oil cooling [17] has also been used.

## 12 Cavity Tuning

We already mentioned in Section 2 that a DC bias current may be used to decrease  $\mu_{\Delta}$  which results in a higher resonant frequency. This is one possible way to realize **cavity tuning**. Strictly speaking, one applies a quasi-DC bias current since the resonant frequency must be modified during a synchrotron machine cycle if it shall be equal to the variable RF frequency. Such a tuning of the resonant frequency  $f_{\text{res}}$  to the RF frequency  $f_{\text{RF}}$  is usually desirable since the large  $Z_{\text{tot}}$  allows to generate large voltages with moderate RF power consumption.

Sometimes, the operating frequency range is small enough in comparison with the bandwidth of the cavity that no tuning is required. This is often the case for MA cavities with sufficiently low Q factors (see Ref. [17]).

If tuning is required, one has at least two possibilities to realize it, bias current tuning or capacitive tuning. The latter may be realized by a variable capacitor (see Refs. [18, 19]) whose capacitance may be varied by a stepping motor. This mechanical adjustment, however, is only possible if the resonant frequency is not changed from machine cycle to machine cycle or even within one machine cycle.

In the case of bias current tuning for ferrite ring cores, one has two different choices, namely **perpendicular biasing** (also denoted as **transverse biasing**) and **parallel biasing** (also denoted as **longitudinal biasing**). Also a mixture of both is possible [20]. The terms parallel and perpendicular refer to the orientation of the DC field  $H_{\text{bias}}$  in comparison with the RF field  $H$ .

Parallel biasing is simple to realize. One adds bias current loops which may in principle be located in the same way as the inductive coupling loop shown in Fig. 3. If only a few loops are present, current bars with large cross sections are needed to withstand the bias current of several hundred amps. The required DC current may of course be reduced if the number  $N_{\text{bias}}$  of loops is increased accordingly (keeping the ampere-turns constant). This increase of the number of bias current windings may be limited by resonances or by the inductance that is allowed for the bias current circuit (to realize the required tuning speed). On the other hand, a minimum number of current loops is usually applied to guarantee a certain amount of symmetry which leads to a more homogeneous flux in the ring cores.

Perpendicular biasing is more complicated to realize; it requires more space between the ring-cores, and the permeability range is smaller than for parallel biasing. The main reason for using perpendicular biasing is that lower losses can be reached (see Ref. [21]). One can also avoid the so-called **Q-loss effect** or **high loss effect**. The Q-loss effect often occurs in ferrites when parallel biasing is applied and if the bias current is constant or varying only slowly. After a few milliseconds, one observes that the induced voltage breaks down by a certain amount even though the same amount of RF power is still applied (see Refs. [22, 23]). For perpendicular biasing, the Q-loss effect was not observed. The Q-loss effect is not fully understood yet. However, there are strong indications that it may be caused by mechanical resonances of the ferrite ring cores induced by magnetostriction effects [24]. It was possible to suppress the Q-loss effect by mechanical damping. For example, in some types of ferrite cavities, the ring cores are embedded in a sealing compound [25] which should damp mechanical oscillations. Not only the Q-loss effect but also further anomalous loss effects have been observed [22].

When the influence of biasing is described, one usually defines an average bias field  $H_{\text{bias}}$  for the ring cores. For this purpose, one may use the magnetic field

$$H_{\text{bias}} = \frac{N_{\text{bias}} I_{\text{bias}}}{2\pi \bar{r}}$$

located at the mean radius  $\bar{r} = \sqrt{r_1 r_0}$ . Of course, this choice is somewhat arbitrary from a theoretical point of view, but it is based on practical experience.

A combination of bias current tuning and capacitive tuning has also been applied to extend the frequency range [26].

### 13 Further Complications for Ferrite Ring Cores

We already mentioned that the effective differential permeability depends on the hysteresis behavior of the material, i.e. on the history of bias and RF currents. It was also mentioned that, due to the spatial dimensions of the cavity, we have to deal with ranges between lumped-element circuits and distributed elements. The anomalous loss effects are a third complication. There are further points which make the situation even more complicated in practice:

- If no biasing is applied, the maximum of the magnetic field is present at the inner radius  $r_i$ . One has to make sure that the maximum ratings of the material are not exceeded.
- Bias currents lead to an  $\rho^{-1}$  dependency of the induced magnetic field  $H_{\text{bias}}$ . Therefore, biasing is more effective in the inner parts of the ring cores than in the outer parts resulting in a  $\mu_{\Delta}$  which increases with  $\rho$ . According to Eq. (3), this will modify the  $\rho^{-1}$  dependency of the magnetic RF field. As a result, the dependence on  $\rho$  may be much weaker than without bias field.
- The permeability does not only depend on the frequency, on the magnetic RF field and on the biasing. It is also temperature-dependent.
- Depending on the thickness and the conductivity of the ring cores, on the material losses and on the operating frequency, the magnetic field may decay from the surface to the inner regions reducing the effective volume.
- At higher operating frequencies with strong bias currents, the differential permeability will be rather low. This means that the magnetic flux will not perfectly be guided by the ring cores anymore. The fringe fields in the air regions will be more important, and resonances may occur.

### 14 Resonant Frequency Control

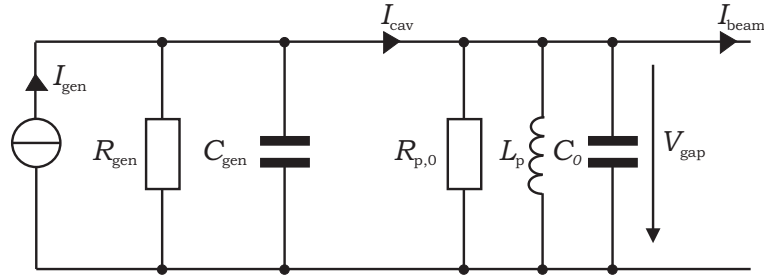


**Fig. 9:** Equivalent circuit of RF generator and cavity.

A method that has traditionally been applied to decide whether a ferrite-loaded cavity is at resonance is the measurement of the phase of the gap voltage and of the phase of the control grid voltage (in case of a tetrode power amplifier).

At first sight it seems to be clear that the cavity is at resonance if and only if the cavity impedance is purely resistive, i.e. if the inductance of the lumped element (parallel) circuit exactly compensates the capacitance (see Fig. 5). Therefore, it is obvious that the generator current and the gap voltage must be in-phase for the cavity operating at resonance.

In order to analyze this fact in detail, however, one should be aware that a tube amplifier also contributes to the overall cavity impedance. Not only the ohmic output impedance will contribute to the overall impedance of the cavity, but also the capacitance of the tetrode (internal) and its circuitry (and also some inductances). As shown in Fig. 9 we may use a model [27] in which the tetrode power amplifier is represented as a voltage-controlled current source with an internal resistor  $R_{\text{gen}}$  in parallel.

The capacitance of the power amplifier is represented by a capacitor  $C_{\text{gen}}$  (if necessary,  $C_{\text{gen}}$  may be frequency-dependent to include the effect of parasitic inductances). The cavity without the power amplifier is shown on the right side of the circuit. It consists of  $R_{\text{p},0}$ ,  $L_{\text{p}}$ , and  $C_0$ . Now it becomes obvious that the resonant frequency of the overall system is

$$\omega_{\text{res}} = \frac{1}{\sqrt{L_{\text{p}}(C_0 + C_{\text{gen}})}}.$$

If the whole cavity system is tuned to resonance, it is not the current  $I_{\text{cav}}$  which is in-phase with the gap voltage  $V_{\text{gap}}$ , but the current  $I_{\text{gen}}$ . This current  $I_{\text{gen}}$  cannot be measured, however, since it may be regarded as an internal current of the tetrode. Fortunately, the control grid voltage  $V_{\text{g1}}$  of the tetrode, however, usually is in phase with the internal current  $I_{\text{gen}}$ . Therefore, a **resonant frequency control** loop may compare the phase of  $V_{\text{g1}}$  with the phase of  $V_{\text{gap}}$ . If both are in phase (or  $180^\circ$  out of phase, depending on the chosen orientation of the voltages), the whole cavity system consisting of generator and cavity will be at resonance. One typically uses a **phase detector** that provides this phase difference between  $V_{\text{g1}}$  and  $V_{\text{gap}}$ . This output signal is then used by a closed-loop controller to modify the bias current of the ferrite cavity such that  $I_{\text{gen}}$  and  $V_{\text{g1}}$  are in phase with  $V_{\text{gap}}$  as desired.

It has to be emphasized that the equivalent circuit in Fig. 5 and the related formulas are still valid. We just have to interpret the circuit in a slightly different way. If we compare it with Fig. 9 it becomes obvious that  $C = C_{\text{gen}} + C_0$  is the total capacitance of generator and cavity, and  $R_{\text{p}} = R_{\text{p},0} || R_{\text{gen}} = \frac{R_{\text{p},0}R_{\text{gen}}}{R_{\text{p},0} + R_{\text{gen}}}$  also includes both contributions.

Sometimes it is desired not to operate the cavity at resonance but slightly off-resonance. In this case, one may choose a target value that differs from zero (or  $180^\circ$ , respectively) for the phase difference.

Completely detuning the cavity may be a choice to de-activate the cavity without having a high beam impedance. Then, of course, no gap voltage is produced so that the closed-loop control system will not work. However, one may modify the bias current in an open-loop mode in this case.

## 15 Cavity Configurations

A comparison of different types of ferrite- or MA-loaded cavities can be found in Refs. [28–30]. We just summarize a few aspects here that lead to different solutions.

- Instead of using only one stack of ring cores and only one ceramic gap as shown in Fig. 3, one may also use more sections with ring cores (e.g. one gap with half the ring cores on the left side and the other half on the right side of the gap — for reasons of symmetry) or more gaps. Sometimes, the ceramic gaps belong to different independent cavity cells which may be coupled by copper bars (e.g. by connecting them in parallel [17]). Connections of this type must be short to allow operation at high frequencies.
- One configuration that is often used is a cavity consisting of only one ceramic gap and two ferrite stacks on both sides. Figure-of-eight windings (for a bias current) surround these two ferrite stacks (see Ref. [31]). With respect to the magnetic RF field, this leads to the same magnetic flux in both stacks. In this way, an RF power amplifier that feeds only one of the two cavity halves will indirectly supply the other cavity half as well. This corresponds to a 1:2 transformation ratio. Hence, the beam will see four times the impedance compared with the amplifier load. Therefore, the same RF input power will lead to higher gap voltages (but also to a higher beam impedance). The transformation law may be derived by an analysis that is similar to the one in Section 3.
- Instead of the inductive coupling shown in Fig. 3, one may also use capacitive coupling if the power amplifier is connected to the gap via capacitors. If a tetrode power amplifier is used, one still has to provide it with a high anode voltage. Therefore, an external inductor (choke coil) is necessary which allows the DC anode current but which blocks the RF current from the DC power sup-

ply. Often a combination of capacitive and inductive coupling is used (e.g. to influence parasitic resonances). The coupling elements will contribute to the equivalent circuit.

- Another possibility is inductive coupling of individual ring cores. This leads to lower impedances which ideally allow a  $50 \Omega$  impedance matching to a standard solid-state RF power amplifier (see Ref. [32]).
- In case a small relative tuning range is required, it is not necessary to use biasing for the ferrite ring cores inside the cavity. One may use external tuners (see Refs. [33, 34]) which can be connected to the gap. For external tuners, both parallel and perpendicular biasing may be applied [35].

No general strategy can be defined how a new cavity is designed. Many compromises have to be found. A certain minimum capacitance is given by the gap capacitance, the power amplifier capacitance, and parasitic capacitances. In order to reach the upper limit of the frequency range, a certain minimum inductance has to be realized. If biasing is used, this minimum inductance must be reached using the maximum bias current but the effective permeability should still be high enough to reduce stray fields. Also the lower frequency limit should be reachable with a minimum but non-zero bias current. There is a maximum RF field  $B_{\text{RF,max}}$  (about  $10 \dots 20$  mT for ferrites) which should not be exceeded for the ring cores. This imposes a lower limit for the number of ring cores. The required tuning range in combination with the overall capacitance will also restrict the number of ring cores. As mentioned above, the amplifier design should be taken into account from the very beginning, especially with respect to the impedance. The maximum **beam impedance** that is tolerable is defined by beam dynamics considerations. This impedance budget also defines the power that is required. If more ring cores can be used, the impedance of the cavity will increase, and the power loss will decrease for a given gap voltage.

## 16 The GSI Ferrite Cavities in SIS18

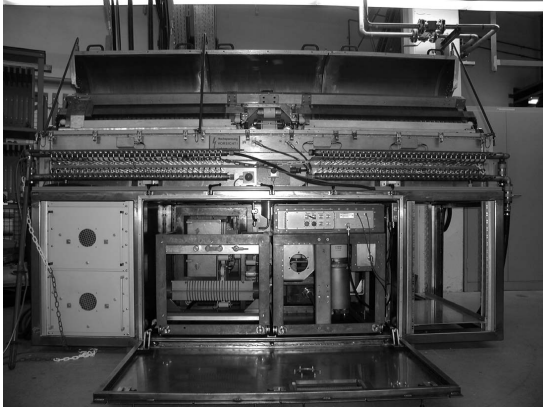


**Fig. 10:** SIS18 ferrite cavity. Photography: GSI Helmholtzzentrum für Schwerionenforschung GmbH, T. Winnefeld.

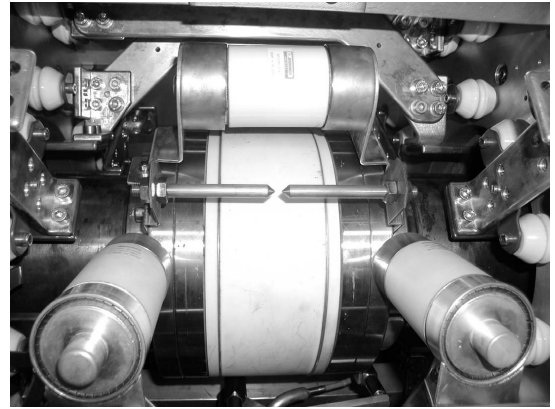


**Fig. 11:** Gap area of the SIS18 ferrite cavity. Photography: GSI Helmholtzzentrum für Schwerionenforschung GmbH, T. Winnefeld.

As an example for a ferrite cavity, we summarize the main facts about GSI's SIS18 ferrite cavities (see Figs. 10 and 11). Two identical ferrite cavities are located in the synchrotron SIS18.

The material Ferroxcube FXC 8C12m is used for the ferrite ring cores. In total,  $N = 64$  ring cores are used per cavity. Each core has the following dimensions:

$$d_o = 2 r_o = 498 \text{ mm}, \quad d_i = 2 r_i = 270 \text{ mm}, \quad d_{\text{core}} = 25 \text{ mm}, \quad \bar{r} = \sqrt{r_i r_o} = 183 \text{ mm}$$

For biasing,  $N_{\text{bias}} = 6$  figure-of-eight copper windings are present. The total capacitance amounts to

**Table 1:** Equivalent circuit parameters for SIS18 ferrite cavities (without resistance of tetrode amplifiers).

<b>Resonant frequency</b> $f_{\text{res}}$	620 kHz	2.5 MHz	5 MHz
<b>Relative permeability</b> $\mu'_{\text{p,r}}$	450	28	7
<b>Magnetic bias field</b> $H_{\text{bias}}$ <b>at mean radius</b>	25 A/m	700 A/m	2750 A/m
<b>Bias current</b> $I_{\text{bias}}$	4.8 A	135 A	528 A
<b><math>\mu'_{\text{p,r}} Qf</math> product</b>	$4.2 \cdot 10^9 \text{ s}^{-1}$	$3.7 \cdot 10^9 \text{ s}^{-1}$	$3.3 \cdot 10^9 \text{ s}^{-1}$
<b>Q-factor</b> $Q_{\text{p,0}}$	15	53	94
$L_{\text{s}}$	88.2 $\mu\text{H}$	5.49 $\mu\text{H}$	1.37 $\mu\text{H}$
$L_{\text{p}}$	88.5 $\mu\text{H}$	5.49 $\mu\text{H}$	1.37 $\mu\text{H}$
$R_{\text{s,0}}$	22.8 $\Omega$	1.63 $\Omega$	0.46 $\Omega$
$R_{\text{p,0}}$	5200 $\Omega$	4600 $\Omega$	4100 $\Omega$
<b>Cavity time constant</b> $\tau$	7.7 $\mu\text{s}$	6.7 $\mu\text{s}$	6.0 $\mu\text{s}$

$C = 740$  pF including the gap, the gap capacitors, the cooling disks, and other parasitic capacitances. The maximum voltage that is reached under normal operating conditions is  $\hat{V}_{\text{gap}} = 16$  kV.

Table 1 shows the main parameters for three different frequencies. All these values are consistent with the formulas presented in this article. It is obvious that both  $\mu'_{\text{p,r}} Qf$  and  $R_{\text{p,0}}$  do not vary strongly with frequency justifying the parallel equivalent circuit. This compensation effect was mentioned at the end of Section 5.

All the parameters mentioned here refer to the beam side of the cavity. The cavity is driven by an RF amplifier which is coupled to only one of two ferrite core stacks (consisting of 32 ring cores each). The two ring core stacks are coupled by the bias windings. Therefore, a transformation ratio of 1:2 is present from amplifier to beam. This means that the amplifier has to drive a load of about  $R_{\text{p,0}}/4 \approx 1.1$  k $\Omega$ . For a full amplitude of  $\hat{V}_{\text{gap}} = 16$  kV at  $f = 5$  MHz the power loss in the cavity amounts to 31 kW.

The SIS18 cavity is supplied by a single-ended tetrode power amplifier using a combination of inductive and capacitive coupling.

It has to be emphasized that the values in Table 1 do not contain the amplifier resistance. Depending on the operating point of the tetrode,  $R_{\text{p}}$  will be reduced significantly in comparison with  $R_{\text{p,0}}$ , and all related parameters vary accordingly.

## 17 Further Practical Considerations

For measuring the gap voltage, one needs a **gap voltage divider** in order to decrease the high-voltage RF to a safer level. This can be done by capacitive voltage dividers. **Gap relays** are used to short-circuit the gap if the cavity is temporarily unused. This reduces the beam impedance which may be harmful for beam stability. If cycle-by-cycle switching is needed, semiconductor switches may be used as gap switches instead of vacuum relays. Another possibility to temporarily reduce the beam impedance is to detune the cavity.

The capacitance/impedance of the gap periphery devices must be considered when the overall capacitance  $C$  and the other elements in the equivalent circuit are calculated. Also further parasitic elements may be present.

On the one hand, the cavity dimensions should be as small as possible since space in synchrotrons and storage rings is valuable and since undesired resonances must be avoided. On the other hand certain minimum distances have to be kept in order to prevent high-voltage spark-overs. Due to **EMC (electromagnetic compatibility)** reasons, RF seals are often used between conducting metal parts of the cavity housing to reduce electromagnetic emission.

In order to fulfill high vacuum requirements, it may be necessary to allow a **bakeout** of the vacuum chamber. This can be realized by integrating a **heating jacket** that surrounds the beam pipe. It has to be guaranteed that the ring cores are not damaged by heating and that safety distances (for RF purposes and high-voltage requirements) are kept.

In case the cavity is used in a radiation environment, the radiation hardness of all materials is an important topic.

## 18 Magnetic Materials

A large variety of magnetic materials is available. Nickel-Zinc (NiZn) ferrites may be regarded as the traditional standard material for ferrite-loaded cavities. At least the following material properties are of interest for the material selection and may differ significantly for different types of material:

- permeability,
- magnetic losses,
- saturation induction (typically 200 . . . 500 mT for NiZn ferrites),
- maximum RF inductions (typically 10 . . . 20 mT for NiZn ferrites),
- relative dielectric constant (in the order of 10...15 for NiZn ferrites but e.g. very high for MnZn ferrites) and dielectric losses (usually negligible for typical NiZn applications),
- maximum operating temperature, thermal conductivity and temperature dependence in general,
- magnetostriction,
- specific resistance (very high for NiZn ferrites, very low for MnZn ferrites).

In order to determine the RF properties under realistic operating conditions (large magnetic flux, biasing), thorough reproducible measurements in a fixed test setup are inevitable [14].

Amorphous and nanocrystalline magnetic alloy (MA) materials have been used to build very compact cavities that are based on similar principles as the classical ferrite cavities (see Refs. [13, 16, 19, 30, 36–41]). These materials have very high saturation induction (500 . . . 1600 mT) [42]. They allow a higher RF induction (provided that cooling is sufficient) and have a very high permeability. This means that a smaller number of ring cores is needed for the same inductance. MA materials typically have lower Q factors in comparison with ferrite materials. Low Q factors have the advantage that frequency tuning is often not necessary (see Ref. [17]) and that it is possible to generate signal forms including higher harmonics [43, 44] instead of pure sine signals. MA cavities are especially of interest for pulsed operation at high field gradients [19, 38, 40]. In case a low Q-factor is not desired, it is also possible to increase it by cutting the MA ring cores to introduce air gaps [16, 38]. The manufacturing process of MA ring cores differs significantly from that of ferrite ring cores [42]. For ferrites, a metal oxide powder is the basis, and sophisticated milling, pressing, sintering and machining/finishing processes are performed. This leads to a homogeneous ring core with a flat surface. In order to produce an MA tape/ribbon, melted metal is disposed on a cooled rotating wheel/drum by means of a nozzle (planar flow casting [42]). The ring core is manufactured by winding the ribbon (including an insulation layer), performing elaborated annealing processes and coating/wrapping/impregnation. Therefore, MA cores are radially inhomogeneous, and the surface is not intrinsically flat. These differences concerning the manufacturing processes are important for cooling considerations (see Section 11) and also for the challenge to control the tolerances of the ring core parameters listed above.

Microwave garnet ferrites have been used at frequencies in the range 40...60 MHz (or even wider) in connection with perpendicular biasing since they provide comparatively low losses (see Refs. [45–49]).

## Acknowledgements

The author would like to thank all the current and former GSI colleagues with whom he discussed several RF cavity issues during the past years, especially Priv.-Doz. Dr. habil. Peter Hülsmann, Dr. Hans Günter König, Dr. Ulrich Laier, Michael Frey, and Dr. Gerald Schreiber. He is also grateful to the former GSI members, especially Dr. Klaus Blasche, Dipl.-Phys. Martin Emmerling, and Dr. Klaus Kaspar for transferring their RF cavity know-how to their successors. Last but not least, the author thanks Dr. Rolf Stassen (FZ Jülich) for reviewing earlier versions of the manuscript and Dr. Ulrich Laier for his helpful comments that led to an improvement of this latest version.

It is impossible to provide a complete list of references. The following list cites only a few references regarding the most important aspects. Many other important publications exist.

## References

- [1] J. M. Brennan. *Handbook of Accelerator Physics and Engineering*, chapter 7.3.8, Ferrite Loaded Cavities, pages 570–572. World Scientific, 1999.
- [2] H. Klingbeil. Ferrite Cavities. In *CAS - CERN Accelerator School: RF for Accelerators, Ebeltoft, Denmark, 8-17 Jun 2010*, pages 299–317, June 2010.
- [3] <http://creativecommons.org/licenses/by/3.0/>.
- [4] H. Klingbeil, U. Laier, and D. Lens. *Theoretical Foundations of Synchrotron and Storage Ring RF Systems*. Springer, Cham, 2014.
- [5] <http://cds.cern.ch/record/1411778/files/p299.pdf>.
- [6] O. Henze, W. M. Rucker, M. Jesenik, V. Goričan, M. Trlep, A. Hamler, and B. Štumberger. Hysteresis model and examples of ferromagnetic materials. *IEEE Transactions on Magnetics*, 39(3):1151–1154, May 2003.
- [7] I. D. Mayergoyz. *Mathematical Models of Hysteresis and their Applications*. Elsevier Science Inc., New York, 2003.
- [8] M. D. Takach and P. O. Lauritzen. Survey of magnetic core models. In *Proceedings of the 1995 IEEE Applied Power Electronics Conference and Exposition - APEC'95*, pages 560–566, 1995.
- [9] F. G. Brockman, H. van der Heide, and M. W. Louwerse. Ferroxcube für Protonensynchrotrons. *Philips Technische Rundschau*, 30(11/12):323–342, 1969/70.
- [10] F. Gerigk. RF Basics I and II. In *CAS - CERN Accelerator School: High Power Hadron Machines, Bilbao, Spain, 24 May-02 Jun 2011*, pages 71–116, May/June 2011.
- [11] F. Pedersen. Beam Loading Effects in the CERN PS Booster. *IEEE Transactions on Nuclear Science*, 22(3):1906–1909, June 1975.
- [12] D. Boussard. Stability Considerations. In *7th LEP Performance Workshop, Chamonix, France*, pages 108–113, Jan 1997.
- [13] M. Kanazawa, T. Misu, A. Sugiura, K. Sato, K. Katsuki, and T. Kusaka. RF Cavity with Co-based Amorphous Core. *Nuclear Instruments and Methods in Physics Research A, NIMA*, 566(2):195–204, October 2006.
- [14] H. Klingbeil, J. Schweickhardt, R. Balß, M. Frey, and P. Hülsmann. Design Process for Synchrotron RF Cavities Loaded With Magnetic Ring Cores. *IEEE Transactions on Nuclear Science*, 67(1):361–368, January 2020.
- [15] S. Papureanu, Ch. Hamm, A. Schnase, and H. Meuth. Performance Test of a Ferrite-Loaded Cavity under Operation Conditions. In *15th IEEE Particle Accelerator Conference, Washington, DC, USA*, May 1993.
- [16] C. Ohmori, E. Ezura, K. Hara, K. Hasegawa, Y. Makida, R. Muto, M. Nomura, T. Ogitsu, T. Shimada, A. Schnase, K. Takata, A. Takagi, F. Tamura, K. Tanaka, M. Toda, M. Yamamoto, and

- M. Yoshii. Development of a high gradient rf system using a nanocrystalline soft magnetic alloy. *Phys. Rev. Special Topics - Accelerators and Beams*, 16:112002–1...8, 2013.
- [17] P. Huelsmann, H. Klingbeil, U. Laier, R. Balss, K.-P. Ningel, B. Zipfel, and Ch. Thielmann. The New Broadband Accelerating System for the SIS18 Upgrade at GSI. In *9th International Particle Accelerator Conference IPAC2018, Vancouver, BC, Canada*, pages 2755–2758, 2018.
- [18] M. Morvillo, R. Garoby, D. Grier, M. Haase, A. Krusche, P. Maesen, M. Paoluzzi, and C. Rossi. The PS 13.3–20 MHz RF System for LHC. In *20th IEEE Particle Accelerator Conference, Portland, OR, USA*, May 2003.
- [19] P. Hülsmann, G. Hutter, and W. Vinzenz. The Bunch Compressor System for SIS18 at GSI. In *EPAC*, pages 1165–1167, 2004.
- [20] C. Völlinger, F. Caspers, and E. Jensen. The Effect of 2-Directional Magnetic Biasing Used for Tuning of a Ferrite-Loaded Re-entrant Cavity. *IEEE Transactions on Nuclear Science*, NS-60(3):2170–2174, December 2013.
- [21] W. R. Smythe and T. G. Brophy. RF Cavities with Transversely Biased Ferrite Tuning. *IEEE Transactions on Nuclear Science*, NS-32(5):2951–2953, October 1985.
- [22] J. E. Griffin and G. Nicholls. A Review of Some Dynamic Loss Properties of Ni-Zn Accelerator RF System Ferrite. *IEEE Transactions on Nuclear Science*, 26(3):3965–3967, June 1979.
- [23] K. Kaspar, H. G. König, and T. Winnefeld. Studies on Maximum RF Voltages in Ferrite-tuned Accelerating Cavities. In *EPAC*, pages 985–987, 2004.
- [24] H. G. König and S. Schäfer. Reduction of Q-Loss-Effects in Ferrite-Loaded Cavities. In *EPAC*, pages 985–987, 2008.
- [25] V. S. Arbuzov et al. Accelerating RF Station for HIRFL-CSR, Lanzhou, China. In *RuPAC XIX, Dubna*, pages 332–334, 2004.
- [26] X. Pei, S. Anderson, D. Jenner, D. McCammon, and T. Sloan. A Wide Tuning Range RF Cavity with External Ferrite Biasing. In *15th IEEE Particle Accelerator Conference, Washington, DC, USA*, May 1993.
- [27] U. Hartel. Modellierung des Regelungs- und Steuerungssystems einer Beschleunigungseinheit für Synchrotrons. Diplomarbeit. Technische Universität Darmstadt, Darmstadt, 2011.
- [28] A. Susini. Low Frequency Ferrite Cavities. In *EPAC*, pages 1416–1417, 1988.
- [29] I. S. K. Gardner. Ferrite Dominated Cavities. In *CAS - CERN Accelerator School: RF Engineering for Particle Accelerators*, pages 349–374, April 1991.
- [30] A. Schnase. Cavities with a Swing. In *CAS - CERN Accelerator School: Radio Frequency Engineering*, pages 236–272, May 2000.
- [31] A. Krusche and M. Paoluzzi. The New Low Frequency Accelerating Systems for the CERN PS Booster. In *EPAC*, 1998.
- [32] J. Dey, I. Kourbanis, and D. Wildman. A New RF System for Bunch Coalescing in the Fermilab Main Ring. In *16th IEEE Particle Accelerator Conference, Dallas, TX, USA*, May 1995.
- [33] R. M. Hutcheon. A Perpendicular-Biased Ferrite Tuner for the 52 MHz PETRA II Cavities. In *12th IEEE Particle Accelerator Conference, Washington, DC, USA*, March 1987.
- [34] C. C. Friedrichs, R. D. Carlini, G. Spalek, and W. R. Smythe. Test Results of the Los Alamos Ferrite-Tuned Cavity. In *12th IEEE Particle Accelerator Conference, Washington, DC, USA*, March 1987.
- [35] R. L. Poirier. Perpendicular Biased Ferrite-Tuned Cavities. In *15th IEEE Particle Accelerator Conference, Washington, DC, USA*, May 1993.
- [36] C. Fougeron, P. Ausset, D. de Menezes, J. Peyromaure, and G. Charruau. Very Wide Range and Short Accelerating Cavity for MIMAS. In *15th IEEE Particle Accelerator Conference, Washington, DC, USA*, May 1993.

- [37] K. Saito, K. Matsuda, H. Nishiuchi, M. Umezawa, K. Hiramoto, and R. Shinagawa. RF Accelerating System for a Compact Ion Synchrotron. In *19th IEEE Particle Accelerator Conference, Chicago, IL, USA*, June 2001.
- [38] C. Ohmori, M. Aoki, Y. Kuriyama, M. Yoshida, Y. Arimoto, M. A. Sato, Y. Kuno, Y. Iwashita, and S. Ninomiya. Ultra-High Field Gradient RF for Bunch Rotation. *Nuclear Physics B (Proc. Suppl.)*, 149:280–282, 2005.
- [39] R. Stassen, K. Bongardt, F. J. Etzkorn, H. Stockhorst, S. Papureanu, and A. Schnase. The HESR RF-System and Tests in COSY. In *EPAC*, 2008.
- [40] L. Mei, Z. Xu, Y. Yuan, P. Jin, Z. Bian, H. Zhao, and J. Xia. MA-core loaded untuned RF compression cavity for HIRFL-CSR. *Nuclear Instruments and Methods in Physics Research A, NIMA*, 661, 2012.
- [41] K. Wang, Z. Xu, P. Jin, X. Fu, Y. Qiao, Y. Cong, X.P. Yi, S.L. Li, R.F. Zhang, X.D. Han, J.C. Yang, J.W. Xia, and H.W. Zhao. Design of the deceleration magnetic alloy cavity for a high-intensity heavy-ion accelerator facility Spectrometer Ring. *Nuclear Instruments and Methods in Physics Research A, NIMA*, 1005, July 2021.
- [42] M. Coey and S. S. P. Parkin. *Handbook of Magnetism and Magnetic Materials*. Springer, Cham, 2021.
- [43] M. Fujieda, Y. Iwashita, A. Noda, Y. Mori, C. Ohmori, Y. Sato, M. Yoshii, M. Blaskiewicz, J. M. Brennan, T. Roser, K. S. Smith, R. Spitz, and A. Zaltsmann. Barrier bucket experiment at the AGS. *Phys. Rev. Special Topics - Accelerators and Beams*, 2:122001–1...14, 1999.
- [44] C. Ohmori, M. Kanazawa, K. Noda, M. Kawashima, T. Misu, Y. Mori, A. Sugiura, A. Takagi, and T. Uesugi. A multi-harmonic RF system using a MA cavity. *Nuclear Instruments and Methods in Physics Research A, NIMA*, 547:249–258, 2005.
- [45] L. M. Earley, H. A. Thiessen, R. Carlini, and J. Potter. A High-Q Ferrite-Tuned Cavity. *IEEE Transactions on Nuclear Science*, NS-30(4):3460–3462, August 1983.
- [46] K. Kaspar. Design of Ferrite-Tuned Accelerator Cavities Using Perpendicular-Biased High-Q Ferrites. Technical report, Los Alamos National Laboratory, New Mexico, USA, November 1984. LA-10277-MS.
- [47] G. Schaffer. Improved Ferrite Biasing Scheme for Booster RF Cavities. In *EPAC*, pages 1234–1236, 1992.
- [48] J. Eberhardt, F. Caspers, and C. Völlinger. Ferrite Characterization for the Design of an Accelerating Cavity With Perpendicular Biasing. *IEEE Transactions on Nuclear Science*, 63(2):693–698, April 2016.
- [49] R. L. Madrak, W. A. Pellico, G. Romanov, C. Y. Tan, and I. Terechkine. Measurements of the Properties of Garnet Material for Tuning a 2nd Harmonic Cavity for the Fermilab Booster. In *Proceedings of NAPAC2016, Chicago, IL, USA*, pages 134–136, 2016.